Modeling of Fouling and Fouling Attachments as a Function of the Zeta Potential of Heterogeneous Membrane Surfaces in Ultrafiltration of Latex Solution

ARTICLE *in* INDUSTRIAL & ENGINEERING CHEMISTRY RESEARCH · JUNE 2014

Impact Factor: 2.59 · DOI: 10.1021/ie501239h

4 AUTHORS:

Amira Abdelrasoul
Ryerson University
27 PUBLICATIONS **31** CITATIONS
SEE PROFILE

H. D. Doan
Ryerson University
63 PUBLICATIONS **629** CITATIONS
SEE PROFILE

Ali Lohi
Ryerson University
118 PUBLICATIONS **862** CITATIONS
SEE PROFILE

Chil-Hung Cheng
Ryerson University
24 PUBLICATIONS **451** CITATIONS
SEE PROFILE

I&EC research
Industrial & Engineering Chemistry Research

Article

pubs.acs.org/IECR

Modeling of Fouling and Fouling Attachments as a Function of the Zeta Potential of Heterogeneous Membrane Surfaces in Ultrafiltration of Latex Solution

Amira Abdelrasoul,* Huu Doan, Ali Lohi, and Chil-Hung Cheng

Department of Chemical Engineering, Ryerson University, 350 Victoria Street, Toronto, Ontario M5B 2K3, Canada

Supporting Information

ABSTRACT: The aim of the present study was to develop a fouling attachment model applicable for both hydrophilic and hydrophobic nonuniform pore size membranes. The predictive models found in the present study allow for an accurate estimation of the depositional and coagulation attachments, at a given operating condition and membrane surface charges. The effect of the zeta potential of the membrane surface on the fouling attachments, the total mass of fouling, the permeate flux, and the specific power consumption in ultrafiltration of a latex solution was also investigated. Polysulfone flat membrane with a MWCO of 60 000 at different surface charges was used under a constant flow rate and cross-flow mode in ultrafiltration of the latex paint solution. Response Surface Methodology (RSM) was implemented throughout the experimental design. Furthermore, hydrophilic ultrafilic and cellulose acetate membranes at different zeta potentials, as well as hydrophobic PVDF membranes, were used to test the reliability and accuracy of the predictive models. The fouling model and the correlations found in the present study form a comprehensive set of predictive models that allow for the estimation of the mass of fouling and the increase in transmembrane pressure, applied to both hydrophilic and hydrophobic membranes of a variety of materials with different molecular weight cutoff (MWCO) values.

1. INTRODUCTION

Pointing at the source of foulant attachment to the membrane's surface is critical when it comes to the research of membrane fouling and its potential practical implementation. There exist two major forces contributing to foulant attachment, specifically: the dispersion interaction force and the polar interaction force.[1] Previous research suggests that foulants that stay attached to the membrane surfaces are most likely caused by the balance of the van der Waals attraction force and the electrostatic repulsion force between particles and the membrane's surface, due to the surface charge. A model hypothesized by Van Oss introduced the concepts of apolar and polar interactions so as to categorize and predict the possible interactions in the aqueous medium. Van Oss based his proposal of apolar and polar interactions in aqueous medium on the Derjaguin, Landau, Verwey, and Overbeek (DLVO) theory.[2] These interactions elucidate the advantage of hydrophilizing the membrane's surface as an effective fouling remediation technique and allowing for a lesser membrane fouling propensity. In order to increase the antifouling properties of the hydrophobic membranes, several methods have been implemented, such as surface coating or surface grafting to increase the membrane hydrophilicity and modification of the membrane surface charge.[3−5] Moreover, the ionic strength of the feed solution was found to significantly alter the surface properties and interactions of the colloidal foulants, which, as a consequence, affected the fouling potential.[6−10] The experimental observation of filtration processes, however, may not be sufficient for a comprehensive understanding of the fouling potential of the latex solution. The relationship between the solution's ionic strength and the zeta potential of the membrane's surface is necessary for the elucidation of the underlying factors affecting membrane fouling and fouling attachments through the particle-to-particle and particle-to-membrane attachments.

As part of this area of research, a variety of empirical and semiempirical models were developed and reported, with two models standing out as the most popular ones: the resistance-in-series model and the concentration polarization model.[11−13] In addition, the permeate flux decline models for the cross-flow ultrafiltration of nonrecycled and recycled systems have also been developed.[14] However, these models are system-specific and are generally inadequate to provide a complete assessment of the effects of the membrane's physical properties on membrane fouling. As a consequence, these models are insufficient in terms of providing accurate process generalization and scale-up. Furthermore, in these models the effects of fouling attachments necessary for a thorough grasp on the mechanisms involved in this phenomenon have not been considered. In most of the studies which applied these models, the monodispersed suspensions were used for the validation purposes. Arguably, this imposes a practical limitation on the extent to which the research results can be applied to real-life cases involving wastewaters and, specifically, wastewaters where the suspended solids have a wide range of particle size distribution.

In the previously conducted study a mathematical model was developed using a homogeneous membrane with a uniform pore size[15] for the ultrafiltration of latex paint solution with a

Received: March 26, 2014
Revised: May 20, 2014
Accepted: May 22, 2014

   dx.doi.org/10.1021/ie501239h | Ind. Eng. Chem. Res. XXXX, XXX, XXX−XXX

wide range of particle size distribution. This mathematical model accounts for the existing chemical attachments in the membrane fouling and incorporates the coupled effects of the chemical and physical factors in membrane fouling, allowing for a comprehensive understanding of the fouling phenomenon and its potential functions. The mathematical model was capable of accurately predicting the increase in the transmembrane pressure and the mass of the fouling retained by the membrane. As was demonstrated in our recent study,[16,17] the fouling attachment probabilities are dependent on the properties of foulants and membranes, operating conditions, and solution chemistry. In addition, a mathematical model that could be applied to heterogeneous membranes with nonuniform pore size was also developed.[18] Predictive models for an accurate estimation of fouling attachments at a given operating condition were recently developed and validated using different types of heterogeneous membranes, with a variety of MWCO values, as illustrated in our previous publication.[19] Nevertheless, a higher level of uncertainty was observed between the mass of fouling and the increase in the transmembrane pressure predicted using the estimated fouling attachment and the experimental values in the case of PVDF hydrophobic membranes. The errors were attributed to the depositional attachment model, which was obtained based on the experimental data of hydrophilic polysulfone membrane with a fixed value of zeta potential of −42.40 mV. Thus, according to this model, the estimated depositional attachment values can only be used for hydrophilic membranes with high negative charges. This indicates that the zeta potential of the membrane surface must be considered to be the predominant factor in ultrafiltation membrane fouling. As a result, it was crucial to introduce the surface charge as zeta potential (ζ) of the membrane surface into our predictive model so as to be generalized for both hydrophilic and hydrophobic membranes. Owing to this, fouling remediation techniques can be developed and applied by manipulating these attachments to reduce the membrane fouling and power consumption.

The objectives of this study are to obtain predictive models that would allow for accurate estimation of the fouling attachments, at a given operating condition, as well as at a specified surface charge of the membrane surface. The fouling attachment models, generalized for hydrophobic and hydrophilic membranes, will be used in turn in the mechanistic fouling model applicable for nonuniform pore size membranes, in order to estimate the mass of the fouling and the increase in transmembrane pressure for the model validations. The effects of the zeta potential of membrane surface on fouling attachments, the total mass of fouling, permeate flux, and specific power consumption in ultrafiltration of the latex solution are also investigated. For the purposes of this study, hydrophilic and hydrophobic membranes of different materials and various MWCO will be used to test the reliability and accuracy of the correlations for applications with nonuniform pore size membranes.

2. ATTACHMENT MATHEMATICAL MODEL

As noted above, a mechanistic model was developed for the deposition of the nonuniform latex particles on heterogeneous, nonuniform pore size membranes.[18] In this model the fouling was considered primarily with respect to the attachments among foulant entities (coagulation attachment) and with respect to the attachments between foulant and the membrane surface (depositional attachment). This mechanistic model was based on the fouling potential mechanisms of different particle sizes getting attached to membrane with nonuniform pore sizes. The primary factors in determining the occurrence of membrane fouling (cake layer formation or pore blocking) and adsorptive internal plugging (pore constriction) were different sizes of latex particles and membrane pores. A heterogeneous membrane had the pore size distribution of (N) nonuniform pore sizes. The range of all potential attachments for every particle size was accordingly applied with the aid of the mathematical model for every available pore size of (i). Eventually, the average percentage (x_i) of each pore size (i), estimated by ImageJ software, was used in the model's calculations. In order to examine the validity and reliability of the model, the monodisperse particles with sizes of 50 and 100 nm and the simulated latex effluent were used. According to these mathematical expressions the mass of the particles contributing to pore blocking can be calculated using eq 1, while the mass of the particles accountable for the cake layer can be estimated using eq 2. Notably, these equations are functions of the membrane's physical properties, feed concentration, particle's projected area, attachment fouling probabilities, and cumulative filtration volume per unit area. The sum of m_p and m_c stands for the total mass of fouling retained by the membrane (m_t).

$$m_p = \sum_{i=1}^{N} x_i \left\{ \frac{\alpha_{pm}\varepsilon_s}{4^{\alpha_{pp}}\sigma_L}\left[1 - \exp\left(-4^{\alpha_{pp}}\sigma_L C_f V_S\right)\right] \right\} + \sum_{i=1}^{N} x_i \left\{ \frac{N_m}{\sigma_{XS}\alpha_{pm}B_i} \left\{ \frac{\pi D_{m_i} L_m B_i \alpha_{pm}}{\tau} - \ln\left[1 + \exp\left(\frac{\pi D_{m_i} L_m B_i \alpha_{pm}}{\tau} - \frac{\sigma_{XS}\alpha_{pm}B_i}{N_m} C_f V_S \right)\right]\right\}\right\} + \sum_{i=1}^{N} x_i \left\{ \frac{\alpha_{pm}\varepsilon_S}{\sigma_S}\left[1 - \exp\left(-\sigma_S C_f V_S\right)\right] \right\} \quad (1)$$

$$m_c = \alpha_{pp} C_f V_s - \left\{ \sum_{i=1}^{N} x_i \left\{ \frac{\alpha_{pm}\varepsilon_s}{4^{\alpha_{pp}}\sigma_L}\left[1 - \exp\left(-4^{\alpha_{pp}}\sigma_L C_f V_s\right)\right] \right\} + \sum_{i=1}^{N} x_i \left\{ \frac{N_m}{\sigma_{xs}\alpha_{pm}B_i} \left\{ \frac{\pi D_{m_i} L_m B_i \alpha_{pm}}{\tau} - \ln\left[1 + \exp\left(\frac{\pi D_{m_i} L_m B_i \alpha_{pm}}{\tau} - \frac{\sigma_{xs}\alpha_{pm}B_i}{N_m} C_f V s \right)\right]\right\}\right\} + \sum_{i=1}^{N} x_i \left\{ \frac{\alpha_{pm}\varepsilon_s}{\sigma_s}\left[1 - \exp\left(-\sigma_s C_f V_s\right)\right] \right\} \right\} \quad (2)$$

where m_p [kg/m^2] is the total mass of particles attached to membrane pores per unit membrane surface area, m_c [kg/m^2] is the total mass of particles in the cake layer per unit membrane surface area, x_i is the average percentage of the pore of size i, N is the number of the nonuniform pore sizes determined in the pore size distribution of the heterogeneous membranes, α_{pp} [dimensionless] is the coagulation attachment probability which represents the particle-to-particle attachment, α_{pm} [dimensionless] is the depositional attachment which represents the particle-to-membrane attachment, ε_s [dimensionless]

dx.doi.org/10.1021/ie501239h | Ind. Eng. Chem. Res. XXXX, XXX, XXX−XXX

is the membrane surface porosity, a [m] is the particle radius, D_{m_i} [m] is the membrane pore diameter of size i, B_i [m^{-2}] is the mass transfer coefficient, σ_L[m^2/kg] is the projected area of a unit mass of the large particles on membrane surface, σ_s [m^2/kg] is the projected area of a unit mass of the small particles on the membrane surface, and σ_{xs} [m^2/kg] is the projected area of a unit mass of the very small particles on the membrane surface. Further details about the classification of the particle sizes were described in Section 2 in our previous study.[18] N_m is the number density of membrane pores per unit membrane surface area, L_m [m] is the length of a membrane pore, τ is tortuosity of the membrane porous structure,[18] C_f [kg/m^3] is the mass concentration of particles in the feed, and V_s [m^3/m^2] is the cumulative volume of the permeate normalized to membrane surface area. The mean average of particle size was used for the projected area calculations for each size range. In addition, the increase in the transmembrane membrane pressure during a filtration process normalized to that of clean membrane can be calculated using eq 3 below:

$$P' = 1 + \frac{1}{1 - \sigma_L \sum_{i=1}^{N} x_i m_{pL_i}} + \frac{1}{1 - \sigma_S \sum_{i=1}^{N} x_i m_{pS_i}} + \frac{1}{\left(1 - \frac{\sum_{i=1}^{N} x_i m_{w_i}}{\rho L_m}\right)^2} + \frac{\hat{R}_c}{R_m}[\alpha_{pp} C_f V_s - (\sum_{i=1}^{N} x_i m_{pL_i} - \sum_{i=1}^{N} x_i m_{pS_i} - \sum_{i=1}^{N} x_i m_{w_i})] \quad (3)$$

where m_{pL_i} [kg/m^2] is the mass of the particles larger than the pore of size i contributing to the pore blocking, m_{w_i} [kg/m^2] is the mass of particles attached to the pore wall of size i, and m_{pS_i} [kg/m^2] is the mass of the small particles contributing to the blocking of the pores of size i. Lastly, R_m [m^{-1}] is the membrane's resistance while $\hat{R}_c$ [m/kg] is the resistance due to the cake layer. As outlined in the previous study,[15] eqs 1 and 2 are solved for α_{pp} and α_{pm} using m_p and m_c values measured experimentally. The fouling attachment model to predict the total mass of fouling and the increase of transmembrane is valid for any period of ultrafiltration time. The experimental design used in the present study provided sufficient data to obtain the required correlations for an accurate prediction of the attachment fouling probabilities using heterogeneous membranes at a given operating condition and is discussed explicitly in Sections 4.3 and 5.3. The mathematical model and these correlations form an entire set of predictive models for the nonuniform pore size membranes.

3. SPECIFIC POWER CONSUMPTION

During the filtration process, the resistance to the permeate flow can be increased due to the pore blockage and the cake layer formation, resulting in the membrane fouling. Hence, the permeate flux noticeably declines with filtration time. A higher permeate flux can be attained by augmenting the transmembrane pressure, which in turn causes a higher energy consumption. The specific power consumption per unit volume of filtrate is defined as

$$\text{Specific power consumption}\left[\frac{\text{kWh}}{\text{m}^3}\right] = 1.916 \times 10^{-6} \times \frac{\overline{\text{TMP}}_{AVG} Q}{\bar{V}_s} \quad (4)$$

where $\overline{\text{TMP}}_{AVG}$ is the time-averaged transmembrane pressure throughout the filtration duration. $\overline{\text{TMP}}_{AVG}$ [psig·min] can be calculated based on the area under the curve, as shown in Figure 1. Q [LPM] is the feed flow rate, and $\bar{V}_s$ [m^3] is the cumulative permeate volume.

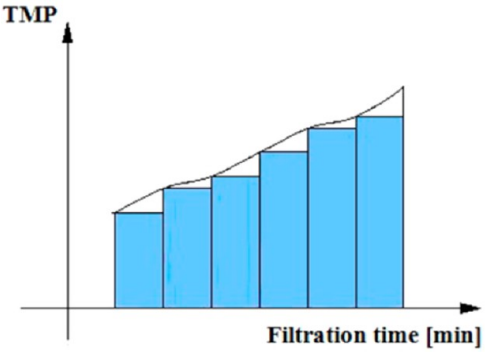

Figure 1. Area under the curve represents $\overline{\text{TMP}}_{AVG}$ [psig·min].

4. MATERIALS AND METHOD

4.1. Experimental Setup and Procedure. A schematic diagram of the experimental setup is shown in Figure 2. A more detailed account about the setup of the experiment, the particulars of the procedure, the membrane filtration unit, and the latex paint used can be found in the previous study.[15] The study[15] reported the details of the procedure to measure the total mass of fouling (m_t), the mass of particles contributing to pore blocking (m_p), and the mass of particles contributing to cake layer (m_c). For the most part, the present study used polysulfone membrane with the chemical structure of $[OC_6H_4OC_6H_4SO_2C_6H_4]_n$, with MWCO of 60 000 (GE Water & Process Technologies). Ultrafilic membrane with MWCO of 100 000 (GE Water & Process Technologies), cellulose acetate (CA) membrane with MWCO of 20 000 (GE Water & Process Technologies), and polyvinylidene difluoride (PVDF) membrane with MWCO of 100 000 (Koch Membrane Systems) were also tested so as to evaluate the predictability and accuracy of the correlations developed for generalized application to a variety of heterogeneous membranes with distinct surface charges. The zeta potentials of the untreated membranes used in the present study were −42.40 mV, −41.50 mV, −2.50 mV, and −33.90 mV for polysulfone, ultrafilic, PVDF, and cellulose acetate membranes, respectively. The membrane surface charge was adjusted using a solution in an MPT-2 autotitrator of the zeta potential analyzer (Zetasizer-Nano Series, Malvern Instruments Ltd., U.K., ±0.01 MV). The zeta potential was adjusted by using 0.1 N H_2SO_4 and 0.1 N NaOH to increase the acidity or the alkalinity of the soaking solution, respectively. Following this adjustment, the membrane sheets were immersed in alkaline or acid solutions for 2 h since this period was optimal for the adsorption of the OH^- or H^+ group on the membrane surface. This time was estimated based on the preliminary experiments for the stability of the surface charge after 25 min of the ultrafiltration process. Polysulfone

dx.doi.org/10.1021/ie501239h | Ind. Eng. Chem. Res. XXXX, XXX, XXX−XXX

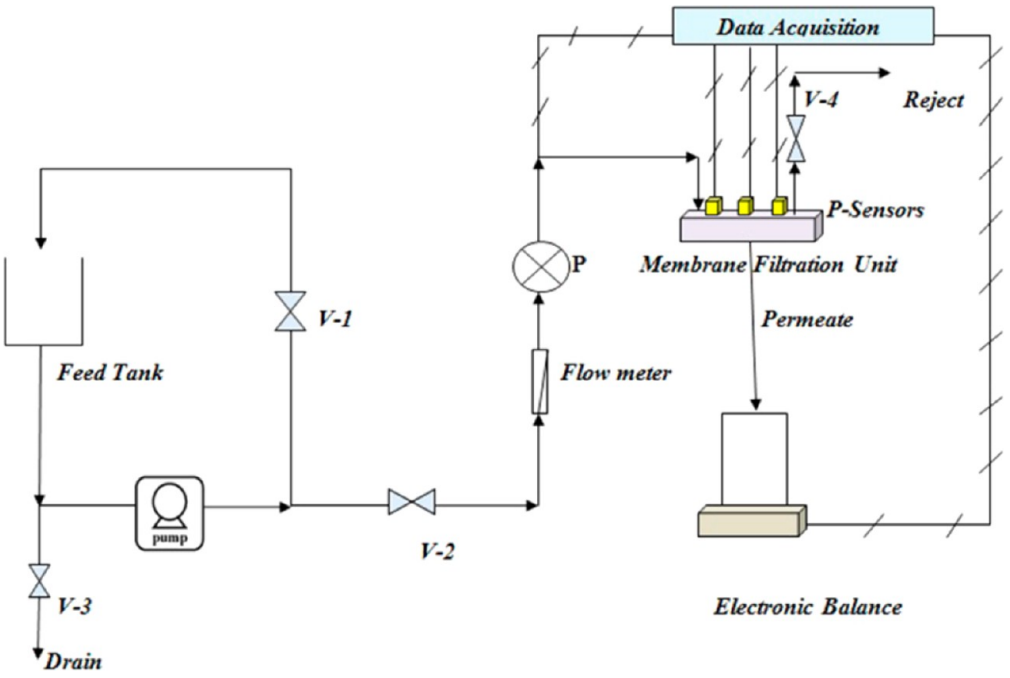

Figure 2. Schematic diagram of experimental setup.

membrane zeta potentials of −10.00 mV, −20.00 mV, −30.00 mV, −40.00 mV, and −50.00 mV were respectively obtained at pH values of 2.4, 4.1, 5.7, 6.8, and 10.9. The ultrafilic membrane with zeta potentials of −15.00 mV and −30.00 mV were obtained at pH values of 2.8 and 6, respectively. Moreover, the zeta potential of the back surface of the membrane sheet was measured after each experimental run of the ultrafiltration process to check the stability of the surface charge of treated membranes. In order to ensure the accuracy of the zeta potential measurement, three identical measurements were performed. This will be discussed in detail in Section 5.2. For these experiments, a simulated latex effluent with a fixed pH value of 7 was used during all of the experimental runs. The zeta potential of latex particles at pH of 7 was approximately −26.61 mV.

4.2. Analytical Methods. A turbidimeter (La Motte 2020 we Turbidimeter, U.S.A., ±2%) was used to measure the turbidity of the permeate for each of the experimental runs. A zeta potential analyzer (ZetasizerNano Series, Malvern Instruments Ltd., U.K., ±0.01 mV) was utilized to measure the zeta potential [mV] of the latex particles and membrane surface. As noted in Section 4.1,[18] the ImageJ software [ImageJ 1.46r, National Institutes of Health, U.S.A.] was used for the estimation of the pore size distributions of heterogeneous membranes. Finally, a detailed account of all the procedures and instruments used for handling solid content, scanning electron microscope SEM, and particle size distribution of latex paint dispersions at different concentrations have been outlined in the previous works.[15]

4.3. Experimental Design and Statistical Method. In the current study, the investigated operational process parameters were transmembrane pressure, feed flow rate, feed concentration, and the zeta potential of polysulfone membrane surface. The solution temperature was maintained constant at room temperature (22−24 °C). Throughout this study, the ultrafiltration time for each experiment was kept constant (25 min), in order to analyze the impact of the operating conditions and the surface charge on fouling attachment probabilities in the experimental design. As a sequence, the influence on the total mass of fouling, cumulative filtration volume per unit area, and specific power consumption could be accurately investigated. In this study, the Central Composite Centered (CCC) Response Surface Method (RSM) was selected as the experimental design method. The coagulation and the depositional attachments are the main responses. The four process parameters of the study include transmembrane pressure, feed flow rate, feed concentration, and zeta potential of the membrane surface. Supporting Information Table S1 presents coded and actual levels of the process parameters. To maintain a high level of accuracy, each process parameter features five levels with four parameter interactions. A total of 30 experiments were performed, and their results were then rigorously analyzed using multiregression. Zero code represents the average range value for each process parameter. In order to minimize the error margin, six replicated experiments at zero code for each process parameter were performed in random order. To determine the best-fitting model of the process of regression and stepwise elimination, a statistical software (Stat-Ease, Version 8.0 Stat-Ease Inc., U.S.A.) was applied. Next, the coefficients for a full model were assessed through regression analysis and then tested for their significance. The F-test was implemented to assess the significance of the coefficients, after which the insignificant coefficients were excluded accordingly. P-value analysis was used to set the level of confidence for the F-test. The coefficients of determination (R^2) and the analysis of variances (ANOVA) were used to evaluate the model fitting.

5. RESULTS AND DISCUSSION

5.1. Effect of the Zeta Potential of Membrane Surface on Membrane Fouling. This study investigates the effect of the zeta potential of the membrane surface on fouling attachments, the total mass of fouling, permeate flux, and specific power concerns. Under the operating conditions of 25 psi, 4.5 LPM, and 1.3 kg/m^3 and after increasing the zeta

dx.doi.org/10.1021/ie501239h | Ind. Eng. Chem. Res. XXXX, XXX, XXX−XXX

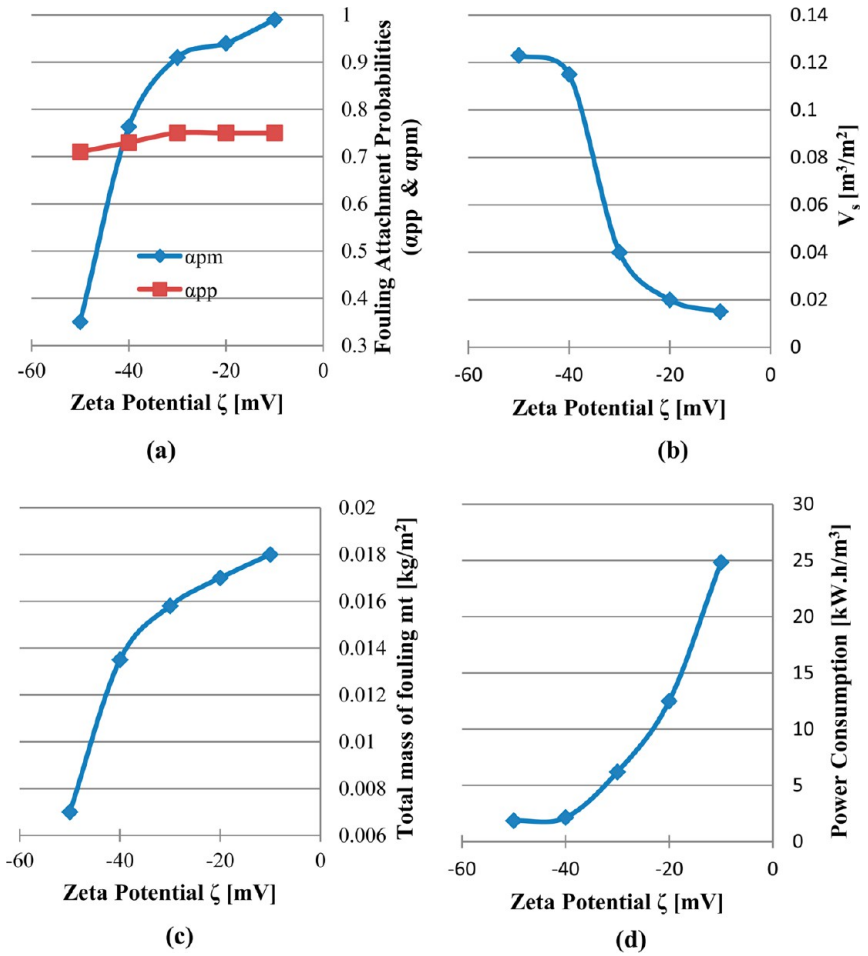

Figure 3. Effect of the zeta potential of polysulfone membrane surface at 25 psi, Q = 4.5 LPM, and C_f = 1.3 kg/m^3 on (a) fouling attachment probabilities (α_{pp}, α_{pm}). (b) Cumulative filtration volume per unit area (V_s) [m^3/m^2]. (c) Total mass of fouling (m_t) [kg/m^2] and (d) specific power consumption [kW·h/m^3].

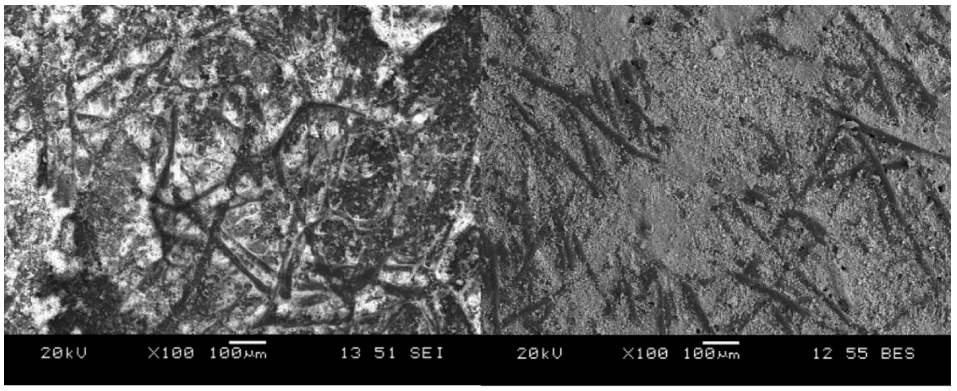

Figure 4. SEM images of polysulfone membranes after ultrafiltration at 25 psi, Q = 4.5 LPM, and C_f = 1.3 kg/m^3. (a) The zeta potential of polysulfone membrane surface −50.00 mV. (b) The zeta potential of polysulfone membrane surface −10.00 mV.

potential of the membrane surface, the surface charge became increasingly negative, from −10.00 to −50.00 mV (5 times), resulted in reduction of depositional attachment (α_{pm}) by 65%, from 0.99 to 0.35, as shown in Figure 3a. This could be attributed to the increased hydrophilicity of the membrane, which was created upon introducing more negative charges on the membrane surface; hence, the electrostatic attraction force between the latex particles and the membrane surface was significantly decreased. The zeta potential of latex particles at pH of 7 is approximately −26.61 mV. The particle-to-membrane attachment was thus significantly reduced because the repulsion forces between latex particles and the higher negativity membrane surface increased. On the other hand, increasing the zeta potential negativity of the membrane surface 5 times resulted in an insignificant decrease of the coagulation attachment (α_{pp}) by 5.3% from 0.75 to 0.71, as shown in Figure

dx.doi.org/10.1021/ie501239h | Ind. Eng. Chem. Res. XXXX, XXX, XXX−XXX

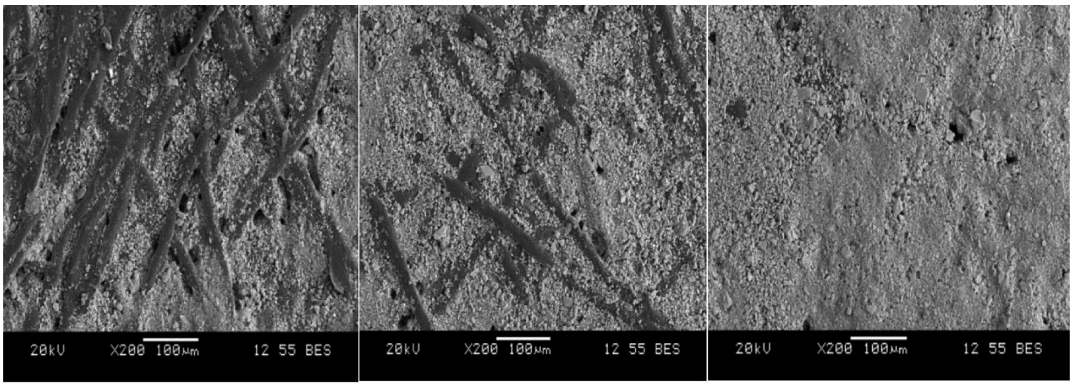

Figure 5. SEM images of ultrafilic membranes after ultrafiltration at 25 psi, Q = 4 LPM, and C_f = 1.3 kg/m^3. (a) Zeta potential of the ultrafilic membrane surface = −41.50 mV. (b) Zeta potential of ultrafilic membrane surface = −30.00 mV. (c) Zeta potential of ultrafilic membrane surface = −15.00 mV.

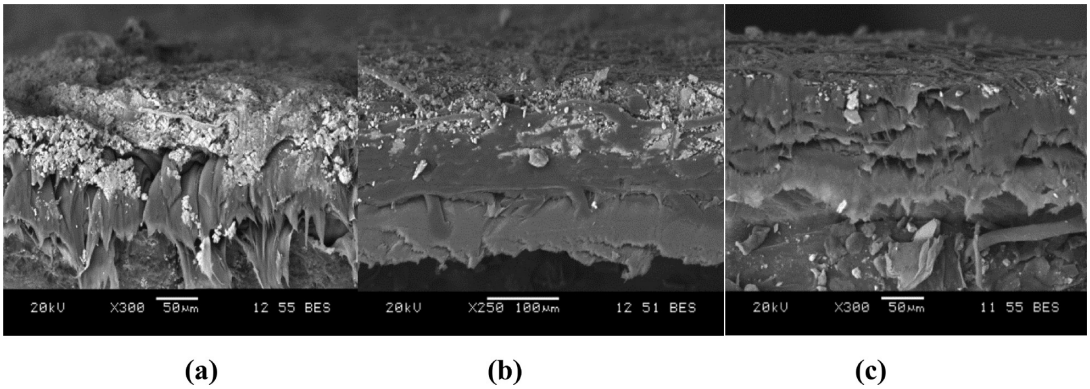

Figure 6. SEM images of polysulfone membrane after ultrafiltration at (a) PS [25 psi], Q = 4.5 LPM, C_f = 1.3 kg/m^3, and −20.00 mV (cross-flow velocity of 46.8 cm/s); (b) PS [25 psi], Q = 7.0 LPM, C_f = 1.3 kg/m^3, and −20.00 mV (cross-flow velocity of 72.8 cm/s); and (c) PS [25 psi], Q = 4.5 LPM, C_f = 1.3 kg/m^3, and −50.00 mV (cross-flow velocity of 46.8 cm/s).

3a. The decrease in the depositional attachment (α_{pm}) caused a significant increase in the cumulative filtration volume per unit area from 0.015 to 0.123 m^3/m^2, an augmentation of about10 times, as shown in Figure 3b. This could be attributed to the significant reduction in the depositional attachment that resulted in less particle attachment to the membrane pores, i.e., less pore blockage to the filtrate passage through the membrane. Moreover, as a consequence of the depositional attachment reduction, the total mass of fouling diminished by 61%, from 0.018 to 0.007 kg/m^2, as illustrated in Figure 3c. Decreasing the total mass of fouling resulted in a lower rate of the transmembrane pressure increase during the filtration process. Accordingly, the specific power consumption was noticeably decreased by 92.5%, from 24.83 to 1.86 kW·h/m^3, as presented in Figure 3d. From these observations a conclusion can be drawn that the depositional attachment is the predominant factor in membrane fouling. In addition, altering the particle-to-membrane attachment (α_{pm}) by manipulating the zeta potential of the membrane surface could be an essential process in fouling remediation.

Figure 4a presents the SEM image of polysulfone membrane with the zeta potential of −50.00 mV after ultrafiltration at a transmembrane pressure of 25 psi, a feed flow rate of 4.5 LPM, and a feed concentration of 1.3 kg/m^3. Alternatively, Figure 4b presents an SEM image of polysulfone membrane with the zeta potential of −10.00 mV after ultrafiltration at the same operating conditions. In SEM images, the white latex particles blocked the membrane pores and deposited between membrane fiber. As shown in Figure 4a, the lower depositional attachment caused a decrease in the total mass of fouling, due to the reduced chances for particles to participate in particle-to-membrane attachment.

It was likewise critical to investigate the effects of increasing the membrane hydrophilicity of different heterogeneous membranes other than polysulfone. For this reason, the effect of the zeta potential of the ultrafilic membrane surface on membrane fouling was investigated at a transmembrane pressure of 25 psi, a feed flow rate of 4 LPM, and a feed concentration of 1.3 kg/m^3, as presented in Supporting Information Table S2. Reducing the negativity of the surface charge of the ultrafilic membrane from the original zeta potential value of −41.50 mV to −30.00 mV resulted in a decreased repulsion force between the membrane surface and latex particles, which in turn caused the depositional attachment (α_{pm}) to increase from 0.70 to 0.85. Higher α_{pm} led to more particle attachment to the membrane surface, resulting in a higher pore blockage, a decrease in the cumulative filtration volume per unit area from 0.123 to 0.115 m^3/m^2, an increase in the mass of fouling from 0.025 to 0.03 kg/m^2, and the power consumption escalation from 1.82 to 1.93 kW·h/m^3. Further decrease in the surface negativity from −30.00 mV to −15.00 mV caused a further increase in the depositional attachment

dx.doi.org/10.1021/ie501239h | Ind. Eng. Chem. Res. XXXX, XXX, XXX−XXX

from 0.85 to 0.96. Consequently, the cumulative filtration volume per unit area decreased from 0.115 to 0.03 m^3/m^2, while the mass of fouling increased from 0.03 to 0.05 kg/m^2. Raising the total mass of fouling caused the increase in the transmembrane pressure to raise at a higher rate through the filtration process, and this allowed the power consumption to increase from 1.93 to 7.5 $kW{\cdot}h/m^3$. It should be noted that the coagulation attachment (α_{pp}) was 0.76, 0.76, and 0.77 using ultrafilic membrane with the zeta potentials of −41.50 mV, −30.00 mV, and −15.00 mV, respectively. Figure 5a−c showcases the SEM images for the ultrafilic membrane after ultrafiltration at a transmembrane pressure of 25 psi, a feed flow rate of 4 LPM, and a feed concentration of 1.3 kg/m^3, at the zeta potentials of −41.50 mV, −30.00 mV, and −15.00 mV, respectively. Figure 5b illustrates that decreasing the negativity of the surface charge of ultrafilic membrane resulted in a smaller number of clean pores, greater number of particle attachments to the membrane surface, and higher chance of particle-to-particle collisions and attachments, if compared to Figure 5a. A further decrease in the surface negativity caused extensive particle deposition on the membrane surface and thus an even higher chance for the particles to contribute to the coagulation attachment and cake formation, as shown in Figure 5c.

For the polysulfone membrane, the difference between the effect of raising the feed flow rate and the effect of increasing the zeta potential of the membrane surface on membrane fouling was also investigated. At a transmembrane pressure of 25 psi, a feed concentration of 1.3 kg/m^3, and a zeta potential of −20.00 mV, increasing the feed flow rate from 4.5 LPM to 7 LPM resulted in a reduced coagulation attachment from 0.75 to 0.55. At the higher flow rate, the cross-flow of the feed can be considered as a continuous washing of the cake layer, causing a decrease in particle-to-particle attachment (α_{pp}). Figure 6b indicates a lower cake height at a cross-flow velocity of 72.8 cm/s (7 LPM), if compared to Figure 6a at a cross-flow velocity of 46.8 cm/s (4.5 LPM). It is worth noting that in the case of the polysulfone membranes it is difficult to measure the cake height accurately due to its heterogeneous multilayered surface. Increasing the feed flow rate resulted in a 41.2% reduction in the total mass of fouling from 0.017 kg/m^2 to 0.01 kg/m^2, owing only to the diminishing of the cake layer. The depositional attachment (α_{pm}) only decreased from 0.94 to 0.89, due to the accumulation of particles trapped inside the membrane tissue, which contributed to the multiple cake layers inside the matrix of the membrane. Moreover, increasing the feed flow rate caused an increase in the cumulative filtration volume per unit area from 0.02 to 0.025 m^3/m^2 (25%). Despite the fact that the total mass of fouling was decreased by 41.2%, thus reduction in transmembrane pressure through the ultrafiltration process from 6.5 to 4 psi, the power consumption per unit volume still increased by 21.7% from 12.5 $kW{\cdot}h/m^3$ to 15.2 $kW{\cdot}h/m^3$. An analysis of these relationships suggests that there is an alignment with the specific power consumption as it is directly proportional to the feed flow rate from eq 4. This proportional correlation entails that the remediation of the fouling is necessary for the reduction of the total mass of fouling in lower flow rates, increase of the cumulative filtration volume per unit area, and a reduction of the power consumption per unit volume of filtrate.

On the other hand, at the transmembrane pressure of 25 psi, feed concentration of 1.3 kg/m^3, and feed flow rate of 4.5 LPM, increasing the surface zeta potential from −20.00 mV to −50.00 mV resulted in a lesser attraction force between the particles and the membrane surface. This caused the depositional attachment (α_{pm}) to noticeably decrease by 62.76%, from 0.94 to 0.35, leading to a smaller number of particles trapped inside the matrix, as presented in Figure 6c. The cumulative filtration volume per unit area escalated more than 5 times from 0.02 m^3/m^2 to 0.123 m^3/m^2, and the total mass of fouling decreased by 58.8%, from 0.017 kg/m^2 to 0.007 kg/m^2. Decreasing the total mass of fouling resulted in a lower increment in the transmembrane pressure through the ultrafiltration process from 6.5 to 1.5 psi. Accordingly, the specific power consumption was significantly reduced by 85.1%, from 12.5 $kW{\cdot}h/m^3$ to 1.8 $kW{\cdot}h/m^3$. The coagulation attachment probability had only slightly lessened from 0.75 to 0.72. Due to a smaller number of particles attached to the membrane surface, chances of collision and attachment of particles on the membrane surface with other particles would be lower, as shown in Figure 6c.

5.2. Stability of the Membrane's Zeta Potential after the Ultrafiltration Process. Polysulfone membrane has an original zeta potential of −42.40 mV. In this study, the 30 experimental runs of CCC experimental design were performed at different zeta potential values of the membrane surface. It was necessary to check the zeta potential of the treated membrane after the ultrafiltration process in order to ensure the stability of the surface charge throughout the filtration process, as depicted in Figure 7.

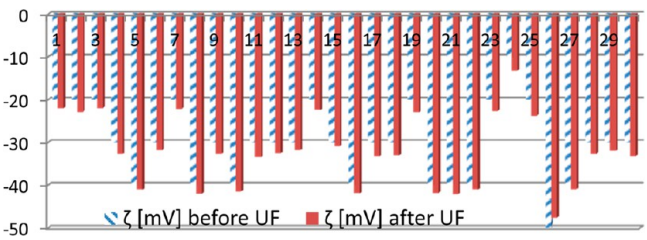

Figure 7. Zeta potential of polysulfone membrane surface before and after ultrafiltration process.

Polysulfone membrane zeta potentials of −10.00 mV, −20.00 mV, −30.00 mV, −40.00 mV, and −50.00 mV were respectively changed to the average zeta potentials of −13.20 mV, −22.50 mV, −32.40 mV, −41.50 mV, and −47.60 mV after the ultrafiltration process. The simulated latex effluent had a pH of 7, which would affect the membrane surface charge during filtration. The zeta potential of polysulfone membrane was −42.40 mV at pH of 7. It was observed that in the case of the treated polysulfone membrane with a lower negativity, whenever the latex solution was allowed to go through the membrane for 25 min, the negativity of the zeta potential of the membrane surface increased by 2.00 to 3.00 mV. On the other hand, for the treated polysulfone membranes with a negativity charge higher than the original zeta potential value, ultrafiltration of latex solution caused a reduction of the negative charge on the membrane surface from −50 mV to −47.6 mV. This can be attributed to the influence of the ionic strength of simulated latex effluent at pH of 7 on the zeta potential of the treated membrane surfaces at higher pH values. Similarly, ultrafilic membrane with zeta potentials of −15.00 mV and −30.00 mV were also changed to −16.50 mV and −31.20 mV, respectively, after 25 min of ultrafiltration with latex solution.

5.3. Statistical Data Analysis. In the current study the Central Composite Centered (CCC) Response Surface

dx.doi.org/10.1021/ie501239h | Ind. Eng. Chem. Res. XXXX, XXX, XXX−XXX

Method (RSM) was selected as the optimal experimental design method. A total of 30 experiments were performed, and the fouling attachment probabilities (α_{pp} and α_{pm}) were calculated for each of the experimental runs, as shown in Supporting Information Table S3. The depositional attachment probability α_{pm} and the coagulation fouling probabilities (α_{pp}) vary between the ranges of 0.35 to 0.99 and 0.22 to 0.98, respectively. On the basis of the ANOVA analysis and the multiregression method, the experimental data of the fouling attachments (α_{pp} and α_{pm}) were found to accurately correspond with the linear model. Equations 5 and 6 provide specific models for the depositional attachment (α_{pm}) and the coagulational attachment (α_{pp}), with the coefficients of determination (R^2) of 95% and 97%, respectively. Notably, the fouling attachment using the polysulfone heterogeneous membranes was not significantly affected by the interaction between the operating conditions.

$$\alpha_{pm} = +0.22 + 0.0528 \times \mathrm{TMP\ [psi]} - 0.0112 \times Q\mathrm{[LPM]} + 0.0804 \times C_f\ [\mathrm{kg/m^3}] + 0.025 \times \zeta\ [\mathrm{mV}] \quad (5)$$

$$\alpha_{pp} = +0.30 + 0.025 \times \mathrm{TMP\ [psi]} - 0.069 \times Q\ [\mathrm{LPM}] + 0.082 \times C_f\ [\mathrm{kg/m^3}] + 1 \times 10^{-7} \times \zeta\ [\mathrm{mV}] \quad (6)$$

The validity of the model coefficients was determined by an ANOVA analysis of the results, as presented in Supporting Information Table S4. The p-value indicates the probability value used to set the level of confidence for the F-test, as well as to ascertain the importance of each coefficient. According to the regression coefficients and probability values (p-value) shown in Supporting Information Table S4, the operating conditions (transmembrane pressure, feed flow rate, and feed concentration) are significantly correlated to both fouling attachments. However, the charge on the membrane surface as represented by the zeta potential value was found to be only significant for the depositional fouling attachment. The zeta potential did not have a substantial effect on the coagulation attachment (particle-to-particle attachment), as confirmed by the experimental data and presented in Section 5.1. On the other hand, increasing the zeta potential of the membrane surface by lowering the negatively charged value resulted in an increased depositional attachment. Therefore, in order to reduce membrane fouling the zeta potential should be decreased by raising the negativity of the surface charge.

The influence of the transmembrane pressure, feed flow rate, and feed concentration on the fouling attachment is shown in Supporting Information Table S3. For example, experimental runs (20 and 21) and (23 and 25) reflect the effect of the transmembrane pressure, and experimental runs (12 and 13) and (17 and 18) indicate the influence of the feed flow rate, while experimental runs (13 and 15) showcase the effects of feed concentration. Either increasing the transmembrane pressure or raising the feed concentrations resulted in an increase in both fouling attachments. On the other hand, an increase in the feed flow rate caused both fouling attachments to decrease. Regression coefficients in eqs 5 and 6 reflect the extent of the impact of each operating condition on α_{pm} and α_{pp} (Supporting Information Table S3). The transmembrane pressure had more impact on the depositional attachment, while the feed flow rate and the feed concentration have more influence on the coagulation attachment, emphasizing and reconfirming the experimental results obtained in our previous work.[19] Accordingly, at constant operating conditions and featuring the same membrane surface charge so as to minimize the attachment probabilities (α_{pm} and α_{pp}) using the polysulfone heterogeneous membranes, the transmembrane pressure and the feed concentration are expected to decrease while the feed flow rate should increase.

Supporting Information Table S3 (runs numbers 7 and 8) shows that, at a transmembrane pressure of 35 psi, feed flow rate of 6 LPM, and feed concentration of 0.78 kg/m^3 and once the surface negativity of polysulfone membrane increased by 100% from −20.00 mV to −40.00 mV, the particle-to-particle attachment only decreased by 2.4%, from 0.82 to 0.80. Moreover, as indicated in Supporting Information Table S3 (runs numbers 26 and 28), at a transmembrane pressure of 25 psi, feed flow rate of 4.5 LPM, feed concentration of 1.3 kg/m^3, and once the surface negativity of polysulfone membrane decreased by 40% from −50.00 mV to −30.00 mV, the particle-to-particle attachment was slightly raised by 2.8% from 0.71 to 0.73. These results suggest that the coagulation attachment is independent of the membrane hydrophilicty. The optimized conditions indicate that the minimum response for both of the fouling attachment probabilities could be obtained at the minimum transmembrane pressure, minimum feed concentration, maximum feed flow rate, and highest negative charge on the membrane surface, within the range of process parameters used in the present study.

5.4. Validation of the Attachment Models with Different Heterogeneous Membranes. This study intended to examine the predictive capability of a complete set of models, including the mechanistic models and the correlations for α_{pm} and α_{pp}, for a variety of operating conditions with various heterogeneous membranes featuring different materials, MWCO values, and surface charges. This analysis was conducted in order to verify the accuracy and reliability of the developed correlations for α_{pm} and α_{pp}. Ultrafilic and PVDF membranes with a MWCO of 100 000 and cellulose acetate membranes with a MWCO of 20 000 were specifically tested for this purpose. Details about the pore size distribution of these membranes were described in Section 4.3 of the previous study.[19]

Supporting Information Table S5 reflects the agreement between the mass of fouling measured experimentally and the value predicted from the mechanistic models using the fouling attachments estimated by the correlations for α_{pm} and α_{pp}. For the polysulfone membrane, the validation experiments were performed over a range of operating conditions rather than the ones used in the experimental design. The mass of fouling measured experimentally corresponded to the value predicted through the fouling attachment predictive models, with the error range of 2.5−9.1% (runs numbers 1−8) and 4.0−14.3% (runs numbers 9−11) for hydrophilic and hydrophobic PVDF membranes, respectively. Admittedly, the complexity of the model's calculation could be responsible for this error, as the model considers each particle size with each pore size, while the real fouling phenomenon features an alternative dynamic that may be executed somewhat differently. As presented in Supporting Information Table S6, in the case of the increase in transmembrane pressure, the experimental values correlated with the values estimated using the fouling attachment predictive models, with error ranges of 7.5−10.0% (run numbers 1−8) and 3.4−12.3% (runs numbers 9−11) for

dx.doi.org/10.1021/ie501239h | Ind. Eng. Chem. Res. XXXX, XXX, XXX−XXX

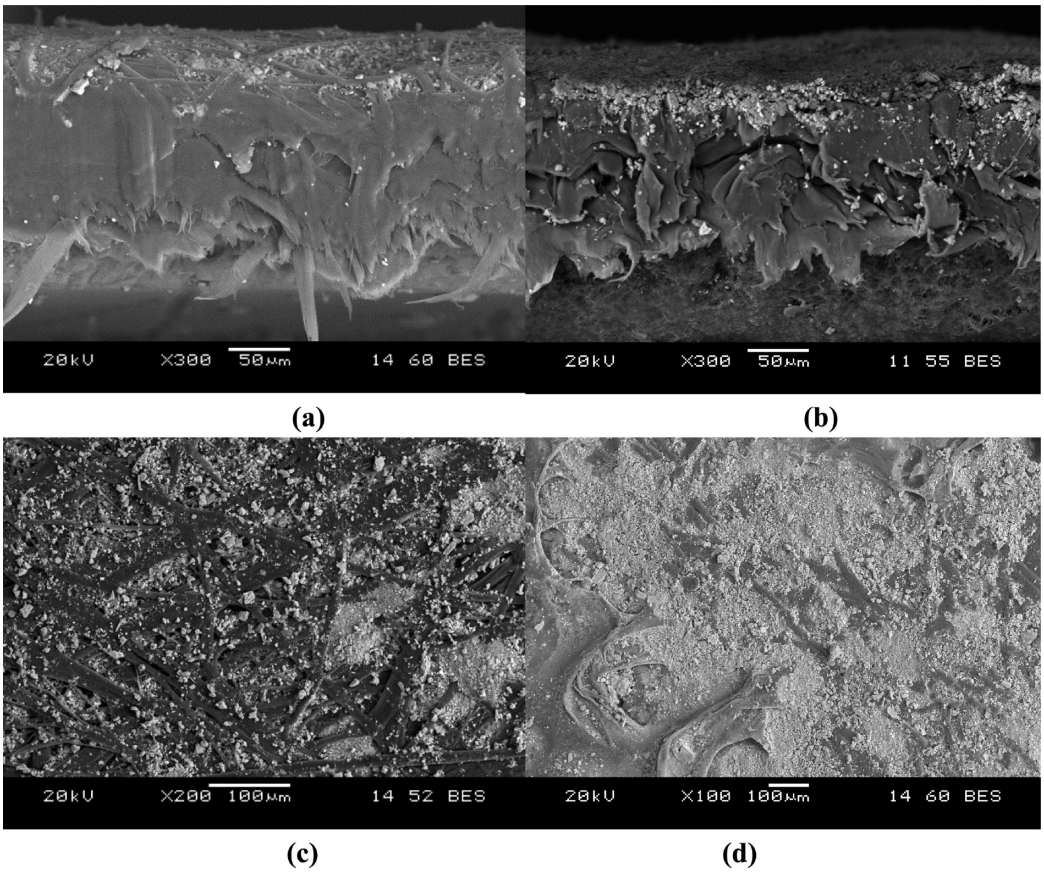

Figure 8. SEM images of membranes after ultrafiltration at Q = 4 LPM and C_f = 0.78 kg/m^3: (a) side view of the cake height of the polysulfone membrane at TMP of 25 psi and zeta potential of −42.40 mV; (b) side view of the cake height of the PVDF membrane at TMP of 15 psi and zeta potential of −2.50 mV; (c) membrane surface of the polysulfone membrane at TMP of 25 psi and zeta potential of −42.40 mV; and (d) membrane surface of PVDF membrane at TMP of 15 psi and zeta potential of −2.50 mV.

hydrophilic and hydrophobic membranes, respectively. Hence, the model prediction of the mass of fouling and the increase in transmembrane pressure agreed quite well with the experimental values for both hydrophilic and hydrophobic membranes.

Equations 5 and 6 illustrate that based on the regression coefficient the transmembrane pressure had more impact on fouling attachment than the hydrophilicity of the membrane. However, the results obtained at the validation runs numbers 3 and 9, in Supporting Information Tables S5 and S6, suggest that the hydrophobic PVDF membrane with the zeta potential of −2.50 mV demonstrated a higher fouling capability at a lower transmembrane pressure than the hydrophilic polysulfone membrane with the zeta potential of −42.40 mV. At the feed flow rate of 4 LPM and the feed concentration of 0.78 kg/m^3, the total masses of fouling were 0.011 kg/m^2 and 0.0125 kg/m^2 after the ultrafiltration process was performed using hydrophilic polysulfone and hydrophobic PVDF membranes at 25 psi and 15 psi, respectively, as shown in Figure 8. The specific power consumption was 14.5 kW·h/m^3 for the polysulfone membrane and 15.4 kW·h/m^3 for PVDF membranes. This could be attributed to the pore size distribution which had a significant effect on the mass of fouling retained by the membrane and caused the increase in transmembrane pressure, as shown in Supporting Information Tables S5 and S6. Increasing the pore size in the case of PVDF membranes with MWCO of 100 000 resulted in greater flow through the membrane pores, if compared to polysulfone membrane of MWCO of 60 000. As a result, the chances for particle-to-particle and particle-to-membrane collisions and attachment increased. Following the growing particle attachment, the total mass of fouling increased at a lower transmembrane pressure, as reflected by the SEM images in Figure 8b,d, as compared to Figure 8a,c. Moreover, the higher negative charge of the polysulfone membrane generated a higher level of repulsion between the particles and the membrane surface and brought about lower depositional attachment (α_{pm}) of 0.34, as compared to 0.97 for the PVDF hydrophobic membrane. On the other hand, the coagulation attachment (α_{pp}) had a higher value in the case of polysulfone membrane due to the impact of the higher transmembrane pressure on particle-to-particle attachment. From this a conclusion can be drawn that the pore size enhances the influence of membrane hydrophilicity more than the impact of the applied transmembrane pressure at same feed flow rate and under the same feed concentration.

Equation 5 presented that the zeta potential would have a stronger effect on the depositional attachment (α_{pm}) than the feed flow rate, while the feed flow rate could be considered the predominant factor in the coagulation attachment (α_{pp}) change, as presented in eq 6. Both equations generated from data with polysulfone membrane and indeed the case for other heterogeneous membranes used in the present study. At transmembrane pressure of 15 psi and a feed concentration of 1.3 kg/m^3, the depositional attachment using polysulfone membrane at feed flow rate of 4 LPM was 0.82, compared to

dx.doi.org/10.1021/ie501239h | Ind. Eng. Chem. Res. XXXX, XXX, XXX−XXX

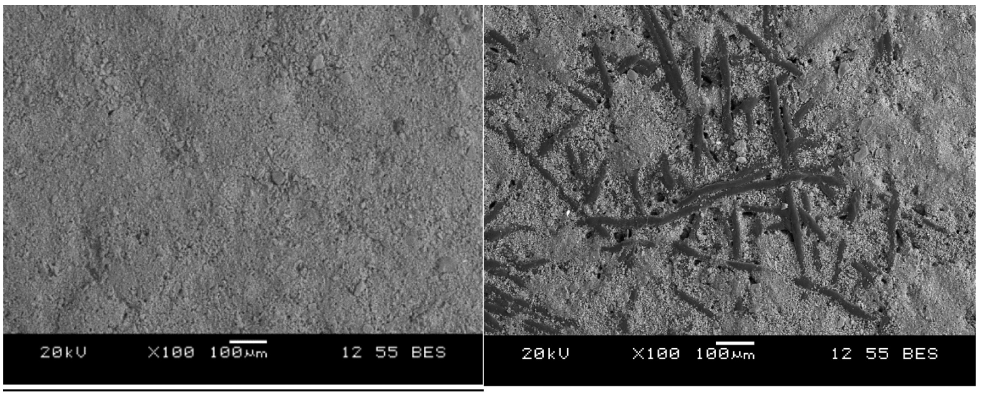

Figure 9. SEM images of membrane surface after ultrafiltration at Q = 7 LPM, TMP = 15 psi, and C_f = 1.3 kg/m^3: (a) PVDF membrane at zeta potential of −2.50 mV; (b) ultrafilic membrane at at zeta potential of −41.50 mV.

0.98 for PVDF membrane at 7 LPM, as shown in Supporting Information Table S5 (Runs 2 and 10). This can be attributed to the ultrafiltration process which is performed using a treated polysulfone membrane with the zeta potential of −10.00 mV, and as a result, causing less of an attraction force between latex particles and the membrane surface, especially if compared to PVDF membrane with the original zeta potential of −2.50 mV. This indicates that at a higher feed flow rate the depositional attachment does not decrease as expected due to the influence of the membrane surface charge. Correlations such as this further confirm that the zeta potential has a greater impact on the depostitioanl attachment than the feed flow rate. On the other hand, the coagulation attachment (α_{pp}) was found to be 0.51 and 0.3 using hydrophilic polysulfone membrane at 4 LPM and hydrophobic PVDF membrane at 7 LPM, respectively. This indicates the fact that the feed flow rate had a significant effect on the particle-to-particle attachment, while the coagulation membrane was functioning independently of the membrane surface charge. PVDF with MWCO of 100 000 allows greater flow through the membrane pores, if compared to the polysulfone membrane of MWCO of 60 000, which resulted in higher chances for particle collisions and attachment. Furthermore, PVDF has a hydrophobic nature with zeta potential −2.5 mV, which increases the chances for greater deposition and higher particle-to-membrane attachment, if compared to polysulfone membrane with zeta potential of −10 MV, as shown in Supporting Information Table S5. However, the total mass of fouling was higher in the case of polysulfone membrane than PVDF, as presented in Supporting Information Table S5. This can be attributed to the influence of feed flow rate which reduced the particle-to-particle attachment and the cake layer.

The effect of hydrophilicty of different membrane materials with the same MWCO on fouling attachments, the total mass of fouling, and the increase in the transmembrane pressure was also investigated at a transmembrane pressure of 15 psi, feed flow rate of 7 LPM, and a feed concentration of 1.3 kg/m^3, using ultrafilic and PVDF membranes of the same MWCO of 100 000. Due to the hydrophilicity of untreated ultrafilic membrane with a zeta potential of −41.50 mV, a depositional attachment of 0.19 was obtained, compared to 0.98 with the hydrophobic PVDF membrane with a zeta potential of −2.50 mV. It is relevant to note that the coagulation attachment (particle-to-particle) was similar for both hydrophilic and hydrophobic membranes (0.29, 0.30), as shown in Supporting Information Table S5. The experimental mass of fouling was 0.0086 kg/m^2 and 0.0134 kg/m^2 for ultrafilic and PVDF membranes, respectively. The transmembrane pressure increased at a higher rate of 5 psi through the ultrafiltration process with the hydrophobic PVDF membrane due to the greater total mass of fouling, in comparison to 2 psi for the hydrophilic ultrafilic membrane (Supporting Information Table S6). Figure 9 reproduces the SEM images of the membrane surface of ultrafilic and PVDF membranes at different surface charges after the ultrafiltration process. The hydrophilic ultrafilic membrane has cleaner pores and a lower total mass of fouling as shown in Figure 9b, compared to the hydrophobic PVDF membrane in Figure 9a at same operating conditions and same MWCO.

Moreover, the experimental run number 3 which performed at low feed concentration of 0.78 kg/m^3, a transmembrane pressure of 25 psi, and feed flow rate of 4 LPM, presented in Supporting Information Tables S5 and S6, was also performed for 15 and 45 min to examine the reliability of the correlations obtained in this study. The results indicated that the mass of fouling predicted from the mechanistic models using the fouling attachments estimated by eqs 5 and 6 were in agreement with the value measured experimentally with the errors of 11% and 14.5% for 15 min and 45 min, respectively, while the predicted increase in transmembrane agreed with the experimental values with the errors of 12.2 and 14.7 for 15 min and 45 min, respectively. The predictive models of fouling attachments demonstrated in our previous work did not focus on the effect of the zeta potential on the membrane surface, as shown in eqs 7 and 8 below:

$$\alpha_{pm} = +0.48 + 0.0056 \times \mathrm{TMP}\ [\mathrm{psi}] - 0.078 \times Q\ [\mathrm{LPM}] + 0.38 \times C_f\ [\mathrm{kg/m^3}] \quad (7)$$

$$\alpha_{pp} = +0.30 + 0.025 \times \mathrm{TMP}\ [\mathrm{psi}] - 0.069 \times Q\ [\mathrm{LPM}] + 0.082 \times C_f\ [\mathrm{kg/m^3}] \quad (8)$$

As shown in Supporting Information Table S7, for the hydrophobic PVDF membrane, the estimated mass of fouling and the increase in the transmembrane pressure using eqs 7 and 8 have noticeably higher error ranges of 26.7% to 43.3% and 25.0% to 41.8%, respectively. It was attributed to the fact that the depositional attachment model was obtained from the

dx.doi.org/10.1021/ie501239h | Ind. Eng. Chem. Res. XXXX, XXX, XXX−XXX

experimental data using hydrophilic polysulfone membrane with zeta potential of −42.40 mV. However, the PVDF membrane is a hydrophobic membrane with a zeta potential of −2.50 mV, which would have a relatively higher attraction force with the latex particles with a zeta potential of −26.61 mV, as compared with other hydrophilic membranes carrying more negative charges, and mentioned in detail in Section 4.3 of the previous study.[19] Therefore, the depositional attachment (particle-to-membrane) estimated from eq 7 can only be implemented for hydrophilic membranes with high negative charges.

The predictive models presented in the present study provide a number of key correlations for the mass of fouling and the increase in the transmembrane pressure applicable to a variety of heterogeneous membranes with different membrane surface zeta potentials, as demonstrated in Supporting Information Tables S5 and S6. Moreover, the models yielded good agreement between predicted values and experimental data even for the PVDF hydrophobic membranes as demonstrated in Supporting Information Table S7. The mass of fouling predicted by the models developed in the present study had a significantly lower error range of 7.8−14.3%, as compared to the range of 26.7−43.3% using eqs 7 and 8 that do not include the effect of the zeta potential of the membrane surface on fouling. Likewise, the increase in the transmembrane pressure error was found within the range of 8.9−12.3%, as compared to 25−41.8%. Hence, the depositional correlation formulated in the present study is applicable for both hydrophilic and hydrophobic membranes.

6. CONCLUSION

The zeta potential of the membrane surface has a predominant effect on the fouling attachment model. The total mass of fouling and the power consumption could be reduced by manipulating the depositional attachment between latex particles and the membrane surface. At the transmembrane pressure of 25 psi and feed concentration of 1.3 kg/m^3, the raising of the polysulfone membrane hydrophilicity from −20.00 mV to −50.00 mV at a lower feed flow rate of 4.5 LPM causes a 58.8% decrease in the total mass of fouling, a 5 times increase in the cumulative filtration volume per unit area, and a 85.1% reduction in the specific power consumption. On the other hand, at the transmembrane pressure of 25 psi, feed concentration of 1.3 kg/m^3, and zeta potential of −20.00 mV, increasing the feed flow rate from 4.5 LPM to 7 LPM brings about the reduction in the coagulation attachment from 0.75 to 0.55, while the depositional attachment lowers only marginally from 0.94 to 0.89. Although the total mass of fouling was decreased by 41.2%, in turn limiting the increase in transmembrane pressure through the ultrafiltration process from 6.5 to 4, the power consumption per unit volume actually increased by 21.7% from 12.5 kW·h/m^3 to 15.2 kW·h/m^3. This indicates that the specific power consumption is directly proportional to the feed flow rate.

The fouling model and the fouling attachment correlations taking into account the effect of the zeta potential on fouling found in the present study form a comprehensive set of predictive models, applicable to both hydrophilic and hydrophobic membranes in a variety of materials with different molecular weight cut off (MWCO) values. The mass of fouling experimentally measured agreed with the predicted value using the fouling attachment models, with the error range of 2.5−9.1% and 4.0−14.3% for hydrophilic and hydrophobic membranes, respectively. For the increase in the transmembrane pressure, the experimental values agreed with the predicted values, with error ranges of 7.5−10.0 and 3.4−12.3% for hydrophilic and hydrophobic membranes, respectively. The hydrophilicity of the membrane did not have a noticeable effect on the particle-to-particle attachment. The effect of zeta potential on depositional fouling attachment was found to be significant, especially for hydrophobic membranes such as PVDF. For PVDF membrane, the predicted mass of fouling calculated using the correlations incorporating the zeta potential effect had a much lower error of 7.8 to 14.3%, as compared to the error of 26.7 to 43.3% using the correlations without the effect of the zeta potential of the membrane surface. Likewise, for the increase in the transmembrane pressure, the error range was 8.9 to 12.3%, as compared to 25 to 41.8% using the models without the effect of the zeta potential. Hence, the depositional correlation found in this study directly agrees with hydrophilic and hydrophobic membranes. The correlations and fouling model proposed in this study form an essential set of predictive models necessary for the estimation of the mass of fouling and the increase in transmembrane pressure, generalized for the applications of hydrophilic and hydrophobic membranes in a variety of materials with varying molecular weight cut off (MWCO) values.

■ ASSOCIATED CONTENT

Ⓢ Supporting Information

Tabulated data of the process parameters, experimental design, statistical analysis, and model agreements. This material is available free of charge via the Internet at http://pubs.acs.org.

■ AUTHOR INFORMATION

Corresponding Author

*Tel: +1 647 929 3491. Fax: +1 416 979 5083. E-mail: amira.abdelrasoul@ryerson.ca.

Notes

The authors declare no competing financial interest.

■ ACKNOWLEDGMENTS

The authors are grateful for the financial support from the Natural Science and Engineering Research Council of Canada (NSERC). The assistance and facilities provided by the Department of Chemical Engineering, Ryerson University, have made this research possible and are also highly appreciated.

■ NOMENCLATURE

a	Particle radius [m]
B_i	Mass transfer coefficient through the pore size i [m^{-2}]
C_f	Concentration of foulants in the feedwater [kg/m^3]
D	Diffusion coefficient of colloidal particles [m^2/s]
D_{m_i}	Membrane pore diameter of size i [m]
L_m	Length of membrane pores [m]
m_p	Mass of particles attaching to membrane pores in a unit membrane surface area [kg/m^2]
m_{pL_i}	Mass of the particles larger than the pore of size i contributing to pore blocking [kg/m^2]
m_{pS_i}	Mass of small particles attaching to membrane pores of size i in a unit membrane surface area [kg/m^2] ($D_{m_i}/6$ < particle size < $D_{m_i}/2$)

dx.doi.org/10.1021/ie501239h | Ind. Eng. Chem. Res. XXXX, XXX, XXX−XXX

m_c Total mass of particles in the cake layer per unit membrane surface area [kg/m^2]
m_t Total mass of particles retained per unit membrane surface area [kg/m^2]
m_{w_i} Mass of the particles attaching to the pore walls of size i normalized to unit membrane surface area [kg/m^2] (particle size < $D_{m_i}/6$)
N Total number of the nonuniform pore sizes determined in the pore size distribution of the heterogeneous membranes
N_m Number density of membrane pores per a unit membrane surface area
TMP Initial transmembrane pressure [psi]
$\overline{TMP}_{AVG}$ Time-averaged transmembrane pressure throughout the filtration duration [psig·min]
P' The increase in transmembrane pressure during filtration normalized to that of clean membranes [dimensionless]
Q Feed flow rate [L/min]
R_m Resistance due to the membrane [m^{-1}]
$\hat{R}_c$ Resistance due to the cake [m/kg]
V_s The cumulative volume of the permeate normalized to membrane surface area [m^3/m^2]
$\overline{V}_S$ Cumulative permeate volume [m^3]
x_i Number-average percentage of the pore of size i
σ Projected area of a unit mass of the particles on membrane surface [m^2/kg]
σ_L Projected area of a unit mass of the large particles (particle diameter ≥ pore diameter) on membrane surface [m^2/kg]
σ_S Projected area of a unit mass of the small particles on the membrane surface [m^2/kg] (pore diameter/6 < particle radius < pore diameter/2)
σ_{XS} Projected area of a unit mass of the very small particles on membrane surface [m^2/kg] (particle radius < pore diameter/6)
ε_s Membrane surface porosity [dimensionless]
α_{pm} Attachment probabilities between a particle and the membrane [dimensionless]
α_{pp} Attachment probabilities between two particles [dimensionless]
τ Tortuosity of the membrane [dimensionless]

REFERENCES

(1) Israelachvili, J. *Intermolecular & Surface Forces*, 2nd ed.; Academic Press Inc.: San Diego, CA, U.S.A., 1992; p 450.
(2) Gregory, J. *Particles in Water: Properties and Processes*; Taylor & Francis Group, CRC Press, 2005; Interaction forces, pp 63−70.
(3) Sui, Y.; Wang, Z.; Gao, C.; Wan, Q.; Zhu, L. An investigation on the antifouling ability of PVDF membranes by polyDOPA coating. *Desalin. Water Treat.* **2012**, *50*, 22−33.
(4) Nikkola, J.; Sievänen, J.; Raulio, M.; Wei, J.; Vuorinen, J.; Tang, C. Surface modification ofthin film compositepolyamidemembrane using atomiclayerdepositionmethod. *J. Membr. Sci.* **2014**, *450*, 174−180.
(5) Zuo, G.; Wan, R. Novelmembranesurfacemodification toenhanceanti-oilfouling propertyformembranedistillationapplication. *J. Membr. Sci.* **2013**, *447*, 26−35.
(6) Singh, G.; Song, L. Quantifying the effect of ionic strength on colloidal fouling potential in membrane filtration. *J. Colloid Interface Sci.* **2005**, *284*, 630−638.
(7) Faibish, R.; Elimelech, M.; Cohen, Y. Effect of interparticle electrostatic double layer interactiosn on permeate flux decline in cross flow membrane filtration of colloidal suspension. *J. Colloid Interface Sci.* **1998**, *204*, 77−86.
(8) Childress, A. E.; Elimelech, M. Effect of solution chemistry on the surface charge of polymeric reverse osmosis and nanofiltration membranes. *J. Membr. Sci.* **1996**, *119*, 253−268.
(9) Mika, M.; Arto, P.; Marianne, N. Effect of pH on hydrophilicity and charge and their effect on the filtration efficiency of NF membranes at different pH. *J. Membr. Sci.* **2006**, *280*, 311−320.
(10) Jones, K. L.; O'Melia, C. R. Protein and humic acid adsorption onto hydrophilic membrane surfaces: effects of pH and ionic strength. *J. Membr. Sci.* **2000**, *165*, 31−46.
(11) Viadero, R. C.; Vaughan, R. L.; Reed, B. E. Study of series resistances in high-shear rotary ultrafiltration. *J. Membr. Sci.* **1999**, *162*, 199−211.
(12) Bruijn, J. P. F.; Salazar, F. N.; Borquez, R. Membrane blocking in ultrafiltration, a new approach to fouling. *Food Bioprod. Process.* **2005**, *83*, 211−219.
(13) Ho, C. C.; Zydney, A. L. Transmembrane pressure profiles during constant flux microfiltration of bovine serum albumin. *J. Membr. Sci.* **2002**, *209* (2), 363−377.
(14) Huanga, J.; Guoa, S.; Zenga, G.; Xionga, Y.; Zhanga, D.; Tanga, X.; Xiea, G. Prediction of fouling resistance and permeate flux in cross-flowmicellar-enhanced ultrafiltration (MEUF). *Colloids Surf., A* **2012**, *401*, 81−89.
(15) Abdelrasoul, A.; Doan, H.; Lohi, A. A mechanistic model for ultrafiltration membrane fouling by latex. *J. Membr. Sci.* **2013**, *433*, 88−99.
(16) Abdelrasoul, A.; Doan, H.; Lohi, A. Impact of operating conditions on fouling probability and cake height in ultrafiltration of latex solution. *J. Membr. Sep. Technol.* **2013**, *2*, 134−147.
(17) Abdelrasoul, A.; Doan, H.; Lohi, A. Effect of pH on fouling attachments and power consumption in ultrafiltration of latex solution. *Can. J. Chem. Eng.* **2014**, *9999*, 1−13.
(18) Abdelrasoul, A.; Doan, H.; Lohi, A.; Cheng, C.-H. Modeling development for ultrafiltratio membrane fouling of heterogeneous membranes with non-uniform pore size, accepted in. *Can. J. Chem. Eng.* **2014**, accepted for publication, manuscript number CJCE-13-0744.
(19) Abdelrasoul, A.; Doan, H.; Lohi, A.; Cheng, C.-H. Modeling of fouling and foulant attachments on heterogeneous membranes in ultrafiltration of latex solution, under review in. *Sep. Purif. Technol.* **2014**, submitted for publication, manuscript number SEPPUR-D-14-00271.